Development of a Multi-Objective Optimization Tool for Intercooled/Recuperated Turboprop Engines for Minimum SFC and Engine Weight

Tacconi, Jacopo; Visser, Wilfried; MacNeil, Rens; Verstraete, Dries

DOI
10.2514/6.2018-4656

Publication date
2018

Document Version
Final published version

Published in
2018 Joint Propulsion Conference

AIAA Propulsion and Energy Forum
July 9-11, 2018, Cincinnati, Ohio
2018 Joint Propulsion Conference

10.2514/6.2018-4656

Development of a Multi-Objective Optimization Tool for Intercooled/Recuperated Turboprop Engines for Minimum SFC and Engine Weight

Jacopo Tacconi* and Wilfried Visser†
Technical University Delft, Delft, 2628CD, The Netherlands

Rens MacNeill‡ and Dries Verstraete§
The University of Sydney, Sydney, NSW, 2006, Australia

The introduction of heat exchangers (HEXs) into turboprop engines can enable higher cycle thermal efficiencies. However, the extra weight associated to the addition of intercooler and/or recuperator could off-set the reduction in specific fuel consumption (SFC). Accurate selection of the effectiveness and pressure losses of the heat exchanger is thus needed to minimize combined engine and fuel weight and to maximize the overall performance. In addition, the choice of other fundamental cycle parameters also influences the heat exchanger behavior. During preliminary design, it thus becomes difficult to quickly evaluate the required trade-off between fuel consumption and weight. The scope of this work is to introduce a multi-objective optimization environment that allows an initial selection and trade-off of optimal cycle parameters for turboprops employing HEXs. Tool demonstration has been given on two different cases of study: a 300hp gas turbine, designed for high altitude UAV applications, and a 100hp turboprop, designed for medium altitudes. Results indicate the effectiveness of the developed environment.

I. Nomenclature

Alt	=	flight altitude
b	=	passage width or burner constant
C	=	compressor absolute velocity
DR	=	diffusion ratio
j	=	Colburn heat transfer factor
J	=	Objective function
K	=	generic constant
L_{ax}	=	impeller axial length
L_v	=	diffuser vane length
$\dot{m}$	=	mass flow
M	=	Mach number
N	=	rotational speed
P_0	=	total pressure
$\%P_{04}$	=	percentage of compressor exit pressure
r	=	radius
r_0/r_1	=	turbine nozzle radius ratio
R	=	gas constant
t	=	blade thickness
T	=	temperature
T_0	=	total temperature
V	=	heat exchanger volume
V_B	=	combustor volume
V_L	=	diffuser vane loading
W	=	Weight or compressor relative velocity
$\dot{W}$	=	power
x	=	design vector
Z_{VD}	=	diffuser vane number
α	=	flow angle
β	=	blade angle or HEX angle of wave pattern
$\Delta P/P$	=	total pressure loss
$\%\Delta$	=	percentage of relative error
ε	=	effectiveness
η	=	efficiency
θ_c	=	compressor diffuser angle
λ	=	compressor work factor
ν	=	impeller/rotor hub to tip radius ratio
ξ	=	cooling flow fraction
Π	=	pressure ratio
ρ	=	density
Ω	=	burner loading

*M.Sc. Student, School of Aerospace Engineering, Propulsion and Power.
†Part-time Lecturer, School of Aerospace Engineering, Propulsion and Power.
‡Ph.D. Student, School of Aerospace, Mechanical and Mechatronic Engineering, AIAA Student Member.
§Senior Lecturer, School of Aerospace, Mechanical and Mechatronic Engineering, AIAA Senior Member.

Subscripts

1 - 2	=	impeller or heat exchanger inlet and exit
3 - 4	=	diffuser or combustor inlet and exit
acc	=	accessories
B	=	burner/combustor
c	=	heat exchanger cold side
C	=	compressor
des	=	design
$gear$	=	gearbox
I	=	compressor impeller
IC	=	intercooler
h	=	heat exchanger hot side
N	=	turbine nozzle
ref	=	reference
RC	=	recuperator
s	=	impeller tip/shroud
sh	=	engine shaft
S	=	compressor or turbine stage
ts	=	total to static
T	=	turbine
θ	=	tangential component

II. Introduction

Engine specific fuel consumption (SFC) has reduced drastically over the last decades, partially due to increases in turbomachinery efficiency and improvements in material capabilities [1–3]. However, this trend is currently leveling-off, and the introduction of heat exchangers (HEXs) is an attractive pathway to further appreciable overall efficiency increments. Nevertheless adding intercoolers and recuperators involves a careful balance to ensure that engine weight and parasitic drag do not off-set any gains in SFC.

Adding heat exchangers is further complicated by the interplay between thermodynamic cycle parameters and heat exchanger performance. Equation (1) [2], for instance, shows that the recuperator matrix volume (and weight) not only depends on heat exchanger design parameters like effectiveness and pressure drop, but is also influenced by the overall cycle pressure ratio.

$$V \propto \underbrace{\frac{\dot{m}}{\sqrt{\Pi_C}}}_{\text{(Power Parameter)}} \times \underbrace{\left(\frac{\varepsilon}{1-\varepsilon}\frac{1}{\sqrt{\Delta P/P}}\right)}_{\text{(Recuperator Parameters)}} \times \underbrace{\left(\sqrt{\frac{f}{j^3}}\frac{1}{\beta}\right)}_{\text{(Surface Geometry)}} \tag{1}$$

On the other hand, choices made on the heat exchanger effectiveness and pressure losses generally affect the engine thermodynamics. To this extent, Stevens et al. [4] have shown that for a given effectiveness the maximum admissible pressure loss is function of the compressor pressure ratio. In particular, to obtain an acceptable thermal efficiency the HEX total pressure drop needs to be kept small at low compressor pressure ratios. Moreover, the highest pressure loss should be located in the cold side, since this affects the overall cycle performance less [4].

Due to these significant mutual interactions, the thermodynamic study requires more extensive trade-offs to find optimal engine settings. The present work demonstrates a multi-objective optimization environment for intercooled and/or recuperated turboprop engines to support this preliminary engine development phase.

The environment consists of an engine cycle solver combined with a routine to define main component geometries and associated weights for different turboprop architectures. A multi-objective optimization algorithm has been coupled with the presented tool for minimum SFC and overall engine weight.

The created model has been employed for the preliminary study reported in reference [5]. For this case study the design and part power characterization of a 300hp (~223.71kW) simple recuperated (RC) and intercooled-recuperated (ICR) gas turbine has been performed for an unconventional high altitude UAV mission. For the second case study reported here, the design environment has been applied to a more conventional 100hp (~74.57kW) UAV engine to demonstrate its flexibility.

III. Modeling and Optimization Environment

The developed model is divided into three main operational sections:

1) thermodynamic cycle analysis,
2) detailed component geometrical and design point performance model,
3) detailed component weight model

Each of these sections is briefly described next, followed by a description of the optimization setup. A more detailed explanation of the developed models can be found in reference [5].

A. Thermodynamic Cycle Analysis

For the thermodynamic analysis of the engine, the Numerical Propulsion System Simulation (NPSS) code has been used [6]. NPSS is built around a set of standard component libraries that can be used to define the engine cycle. Furthermore, it uses a built-in modified Newton-Raphson solver to solve for the design point, off-design and transient engine behavior. Each component library is accessible and can be modified by the user.

1. Intercooled-Recuperated Cycle Architecture

For the current work, a conventional single shaft intercooled-recuperated architecture has been modeled in NPSS (Fig. 1). The recuperated engine is simulated using the same model with a zero heat input for the intercooler. Only design point and off-design steady state modes have been considered in the optimization tool reported here.

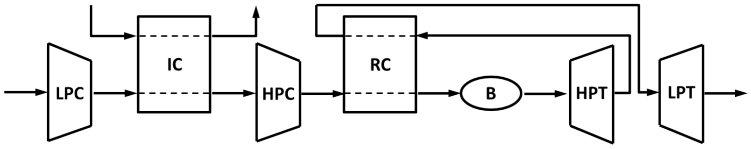

Fig. 1 ***Single shaft intercooled/recuperated gas turbine model***

Standard NPSS elements have been used for off-design performance with exception of intake, heat exchangers and combustor. As described later, these components have been modified to include simple performance equations to better characterize their off-design behavior. While the standard scaled maps have been used for the turbomachinery components, NPSS is coupled with detailed design point performance models so that the turbomachinery efficiencies reflect size and pressure ratios of the components.

The updated NPSS elements are used to build the thermodynamic model from the component libraries available within the program. Figure 2 demonstrates the intercooled/recuperated cycle model as implemented in NPSS. A single shaft arrangement connecting two compressors and two turbines has been assumed for the case studies under examination here. However alternative engine configurations can easily be explored.

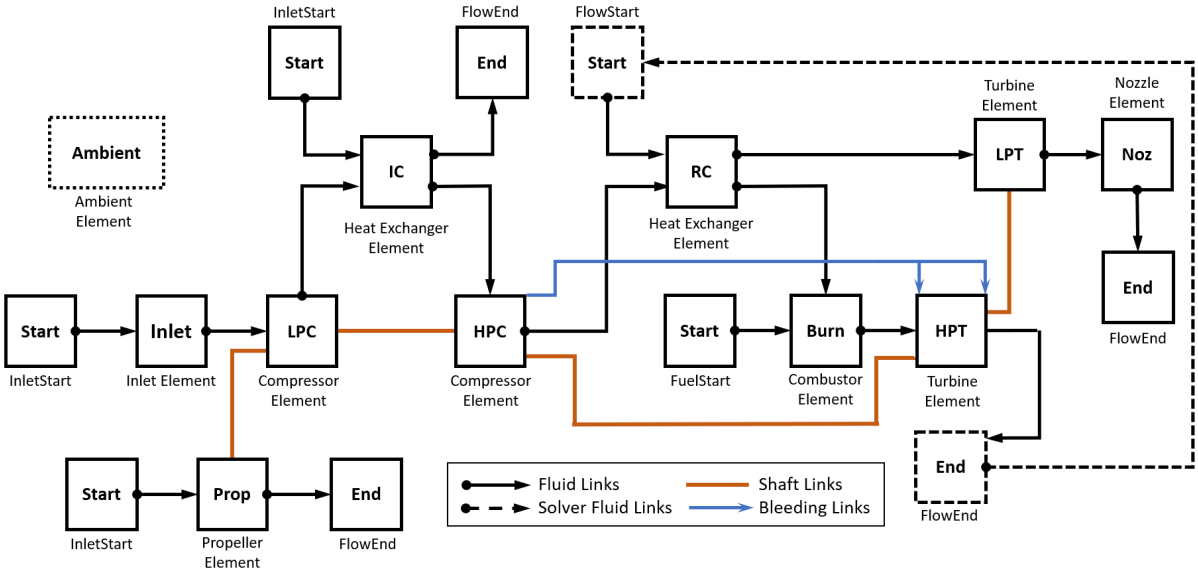

Fig. 2 RC/ICR engine schematic as realized in NPSS

As shown, standard NPSS flow and shaft linking ports have been used to ensure the flow continuity and the turbomachinery mechanical coupling with the propeller element. Because NPSS initializes the engine model from inlet to outlet, it requires knowledge of the inlet flow condition of each element to proceed with the calculations. In non

recuperated engines, this condition is automatically satisfied since the inlet flow conditions of the subsequent element are known once the previous element has been initialized. However, in recuperated engines, this is not the case as the recuperator hot side inlet flow condition can only be defined after the high pressure turbine (HPT) has been solved.

For this reason, a fluid link has been created between the HPT and the recuperator by means of the NPSS solver. This fluid link iteratively ensures that fluid proprieties at the hot side of the HEX are consistent with the turbine exit data (Fig. 3). More detailed information on the actual implementation is available in reference [5].

2. Bleed/Cooling Model

Turbine cooling should be employed for turbine inlet temperatures (TITs) greater that 1250K to avoid a significant reduction in the overall component life [7]. Even though complex cooling methodologies have been developed for radial turbines [8, 9], the most effective cooling procedure still remains film cooling [10].

Using the bleed ports defined within the NPSS compressor and turbine elements, a simple cooling model has been built for input TITs higher than 1250K. The compressor bleed flow has been taken from the HPC exit point to ensure that sufficient pressure is available to cool the HPT stator and rotor. Only the stator cooling flow has been assumed to contribute to the turbine power output.

Equation (2) [11–13] has been used to define the cooling flow requirements for HPT stator and rotor. Where K is a constant set to 0.05 for stator [11, 12], and to 0.2 for the rotor [10]. The cooling effectiveness has been calculated using Eq. (3), assuming the wall temperature equal to the maximum allowed and HPC exit temperature as cooling temperature.

$$\xi = \frac{\dot{m}_{cool}}{\dot{m}} = K \frac{\varepsilon_{cool}}{1 - \varepsilon_{cool}} \tag{2}$$

and

$$\varepsilon_{cool} = \frac{T_{gas} - T_w}{T_{gas} - T_{cool}} \tag{3}$$

Once the required cooling flow has been calculated, the uncooled turbine efficiency is adjusted for cooling losses according to Eq. (4) [11] where a value of 0.125 is used for the constant K_c [11]. More detailed information on the actual NPSS model implementation is available in [5].

$$\frac{\Delta\eta_S}{\eta_S} = -K_c \xi \tag{4}$$

B. Design Point Component Modeling

Detailed component models have been created for compressors, turbines, and combustion chambers. For each of these components, different models have been investigated so that the effects of cycle thermodynamic parameters are adequately correlated to the geometrical and performance characteristics of the component. Feasibility aspects have been also included in the component model to limit the optimization search path to an attainable region.

For the case studies reported here radial turbomachinery components have been selected, based on specific speed (n_s) and specific diameter (d_s), pressure ratios and power involved. For turbomachinery components, the meanline approach discussed by Whitfield and Baines [14], has been preferred with respect to common scaling techniques as this more accurately captures variations in efficiency with pressure ratios and rotational speeds. Meanline approaches additionally provide sufficient geometrical insight to estimate the resultant component weight. The selected design point models for the compressor, turbine and combustor are described next.

1. Centrifugal Compressor

The centrifugal compressor model provides NPSS with an accurate estimation of the compressor efficiency and weight and dimensions. To build the compressor model the component is split into an impeller, a vaneless diffuser section (VLD), and a vaned diffuser (VD). The geometry of the impeller and diffuser is estimated using the procedure presented in [14, 15] and [16, 17] respectively. This geometrical model is then linked to an empirical loss model to estimate the impeller and stage efficiency of the resulting design.

Three loss models have been identified in literature as the most suitable for the intended analysis: Galvas [16, 18], Oh [19] and Aungier [20, 21]. Different compressor losses can be captured by means of these models, as shown in table 1. The Galvas loss model has been selected due to the observations reported in [22]. Underlined advantages of the loss

model are: good performance around the design point and limited amount of geometrical data needed to characterize the compressor efficiency. Corrections have been applied for modeling the effects of shock losses (Aungier [20, 21]), which can become significant at high rotational speeds.

Table 1 Impeller loss model comparison [22]

	Loss	Galvas	Oh	Aungier
External	Recirculation	•	•	•
	Disk Friction	•	•	•
	Leakage		•	•
Internal	Incidence	•	•	•
	Skin Friction	•	•	•
	Blade Loading	•	•	•
	Clearance	•	•	•
	Exit Mixing		•	•
	Shock			•
	Choking			•
	Distortion			•

As shown in Fig. 3, several iterations are needed between the impeller/diffuser geometry building blocks and the loss model to properly refine the initially guessed impeller and stage total to total efficiency values, necessary to start the compressor meanline analysis [14].

The final compressor design then has to be assessed for aerodynamic feasibility. Many authors have associated high diffusion ratios (Eq. (5)) with impeller surge [14, 15]. In particular, Harley [22] uses a diffusion ratio (DR) value of 2.4 to model the inception of surge in his study, whereas, Rodgers [23] suggests values around 1.9 and 2.0. The latter value has been used in this work as the maximum threshold for the aerodynamic acceptability of the compressor impeller.

$$DR = \frac{W_{1s}}{W_2} = \frac{r_{1s}/r_2}{(1 - 2\lambda + \lambda^2/\sin^2\alpha_2)^{1/2}\sin\beta_{1s}} \tag{5}$$

Moreover, reference [17] suggests limiting criteria for the vaned diffuser equivalent divergence angle ($2\theta_c \leq 11°$), and for the vane loading parameter ($V_L \leq 1/3$), defined in Eq. (6). These limitations ensure that diffuser stall is avoided and that the maximum pressure recovery is achieved. Any compressor input combination that results into an aerodynamically infeasible design is penalised so that the optimizer steers away from the design region.

$$V_L = \frac{2\pi(r_3 C_{\theta 3} - r_4 C_{\theta 4})}{Z_{VD} L_v (C_3 - C_4)} \tag{6}$$

The compressor design model has been validated with existing compressor data. A maximum of 5% error on the calculated efficiency has been considered acceptable for the preliminary design intent of the developed tool. Table 2 summarizes the validation outcome, showing that the predicted impeller and stage efficiencies are well within the prefixed tolerance.

Table 2 Compressor model validation

Reference	$\dot{m}$ (kg/s)	N (RPM)	Π_C	η_I	$\eta_{I,ref}$	%Δ	η_S	$\eta_{S,ref}$	%Δ
Japikse and Baines [24]	5.320	14000	2.05	0.919	0.920	0.102	0.870	0.870	0.007
NASA-TN-D-5761 [25]	0.278	38500	2.43	0.911	0.896	1.648	0.823	0.813	1.060
NASA-TM-X-3552 [26]	0.996	68840	5.93	0.877	0.871	0.694	0.783	0.780	0.419
ASME-GT-2002-30394 [27]	2.550	50000	5.10	0.828	0.840	1.449	0.818	0.800	2.297

As mentioned earlier compressor off-design modeling has been performed using common scaling rules defined within NPSS. Off-design calculations are based on the centrifugal compressor map provided in reference [28].

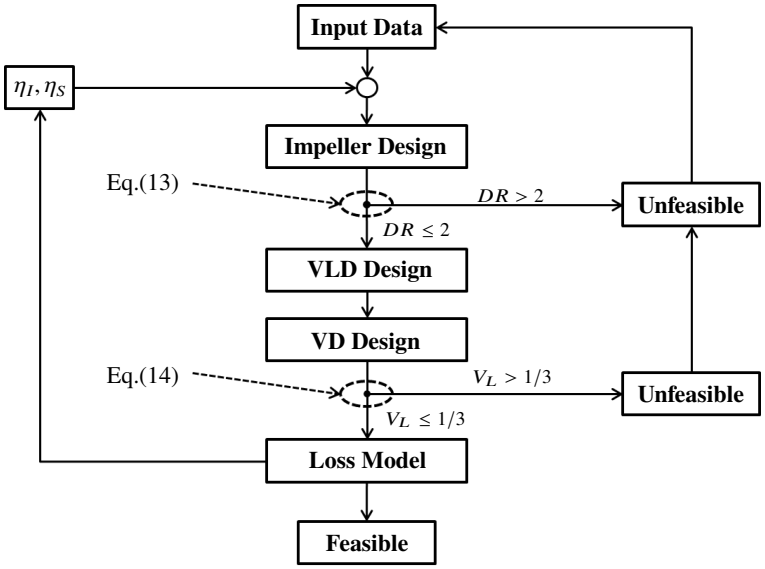

Fig. 3 Centrifugal compressor design diagram

2. Radial Turbine

For the radial turbine a model has been built for the turbine stator and rotor. Primary geometrical features of the turbine are determined from the design procedure discussed in [14, 29]. The resulting geometrical tool is subsequently coupled with a loss model to estimate the stage total to total efficiency. As for the compressor several iterations are needed to ensure proper performance and geometrical matching. Figure 4 summarizes the turbine design procedure.

Two loss models were considered for the radial turbines. The first model was proposed by Rohlik [30, 31], while the second was presented by Glassman [32, 33]. Both models divide the overall turbine losses into the following major contributions: stator losses and rotor incidence losses, passage losses, disk friction losses, clearance losses and kinetic energy losses. Baines [34] has more recently published a slightly modified version of the original Glassman's equations for passage and clearance losses.

Validation has been performed in a similar manner to that of the compressor. The calculated performance of all three loss models has been compared to reference data. The results of this analysis are summarized in Table 3. Variables related to each loss model have been indicated using the initials of the main developing author. The efficiencies reported are expressed as total to static, unless otherwise specified.

Table 3 Turbine model validation

Reference	$\dot{m}$ (kg/s)	N (RPM)	$\dot{W}_T$ (W)	η_R	$\%\Delta_R$	η_G	$\%\Delta_G$	η_B	$\%\Delta_B$	η_{ref}
Khader [35]*	0.080	130000	18020	0.829	1.086	0.840	0.203	0.813	2.936	0.838
Ventura et al. [36]	0.227	38500	22371	0.825	4.456	0.784	0.810	0.808	2.253	0.790
NASA-TP-1730 [37]	0.892	70000	305620	0.823	1.343	0.839	0.576	0.803	3.729	0.834

As for the compressor an accuracy of 5% is deemed satisfactory for the preliminary designs reported here. Although the model accuracy varies from case to case, each of the models satisfies the desired tolerance. As the Glassman loss model results in the most accurate matching for the various turbines, this model has been chosen for the radial turbine design point analysis of this work. As for the compressor, off-design is calculated using a standard scaling approach based on a reference turbine map from [38].

*The efficiencies reported on this row have been expressed as total to total adiabatic in agreement with the reference data [35].

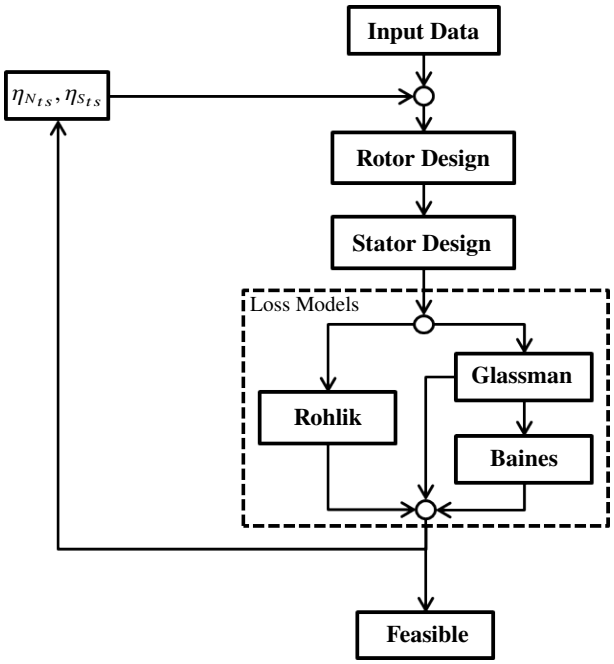

Fig. 4 Radial turbine design diagram

3. Combustor

The combustor has been modeled following the preliminary design techniques presented in ref. [39]. For this component, the model helps to track combustor dimensions and feasibility as function of inlet temperature and mass flow. After all, due to presence of the recuperator, it is important to understand if the inlet air used to cool the combustor liner is sufficient to ensure a feasible solution. Although simplifications have been made, the model has helped to identify thermodynamic inputs that lead to unfeasible combustor design solutions and to properly constrain the associated optimization variables. A complete description of the model is given in ref. [5].

C. Off-design Performance models

While standard component map scaling techniques are used for the compressor and turbine, standard NPSS off-design models have been updated for the intake, the heat exchangers, and the combustion chamber. The heat exchanger and combustor off-design models are briefly described next. For the intake, the pressure recovery factor variations with flight Mach number are modeled after [40, 41].

1. Heat Exchangers

As explained by McDonald [3], the heat exchanger effectiveness normally increases for off-design flow conditions, with the exception of very low mass flow rates where longitudinal conduction effects start to dominate. On the other hand, the hot and cold side pressure loss variation in off-design is much more dependent on inlet flow conditions [42]. Since the availability of complete heat exchangers maps is rare in early design stages, reference [42] has developed a set of equations to model the intercooler and recuperator behavior in off-design. Equation (7) represents a good first order approximation of the recuperator effectiveness change.

$$\varepsilon = 1 - \frac{\dot{m}_{1c}}{\dot{m}_{1c,des}}(1 - \varepsilon_{des}) \tag{7}$$

According to [42], the recuperator cold side pressure losses tend to rise in off-design as consequence of the increased heat transfer, whereas the pressure drop on the hot side normally reduces due to the lower corrected mass flow. Equations (8) and (9) [42] are therefore used to model the recuperator part power pressure losses.

$$\left(\frac{\Delta P}{P}\right)_c = \left(\frac{\Delta P}{P}\right)_{c,des} \cdot \frac{\left[\left(\frac{\dot{m}_{1c}}{P_{01,c}}\right)^2 \cdot \frac{T_{02,c}^{1.55}}{T_{01,c}^{0.55}}\right]}{\left[\left(\frac{\dot{m}_{1c}}{P_{01,c}}\right)^2 \cdot \frac{T_{02,c}^{1.55}}{T_{01,c}^{0.55}}\right]_{des}} \tag{8}$$

and

$$\left(\frac{\Delta P}{P}\right)_h = \left(\frac{\Delta P}{P}\right)_{h,des} \cdot \frac{(\dot{m}_{1h}^2 \cdot T_{01,h})}{(\dot{m}_{1h}^2 \cdot T_{01,h})_{des}} \tag{9}$$

Since the hot side inlet flow condition have a much stronger influence on the intercooler off-design performances, the effectiveness and hot pressure loss equations have to be modified [42]. Equations (10) and (11) have to be respectively used for the intercooler modeling.

$$\varepsilon = 1 - \frac{\left(\frac{\dot{m}_{1h}\sqrt{T_{01,h}}}{P_{01,h}}\right)}{\left(\frac{\dot{m}_{1h}\sqrt{T_{01,h}}}{P_{01,h}}\right)_{des}} (1 - \varepsilon_{des}) \tag{10}$$

and

$$\left(\frac{\Delta P}{P}\right)_h = \left(\frac{\Delta P}{P}\right)_{h,des} \cdot \frac{\left(\frac{\dot{m}_{1h}^2 T_{01,h}}{P_{01,h}^2}\right)}{\left(\frac{\dot{m}_{1h}^2 T_{01,h}}{P_{01,h}^2}\right)_{des}} \tag{11}$$

2. Combustor

The combustor normally exhibits an almost ideal behavior at design conditions, with an efficiency level close to 100%. However, during off-design idle operations and at very high altitudes, the burner efficiency may differ significantly from the design specifications. Reference [43] has correlated the off-design efficiency variation as function of the Ω-parameter (or burner loading) defined according to Eq. (12).

$$\Omega = \frac{\dot{m}_3}{P_{03}^{1.8} \exp(T_{03}/300) V_B} \tag{12}$$

The logarithmic relation given as Eq. (13) well approximates the off-design combustor behavior. The part load constant typically assumes the value of 1.6 [43].

$$\log(1 - \eta) = \log(1 - \eta_{des}) + b \cdot \log\left(\frac{\Omega}{\Omega_{des}}\right) \tag{13}$$

The combustor off-design pressure losses have been defined idealizing the combustor as a duct [43]. This approach is reasonable at the early design stage because the combustor pressure losses are primarily caused by friction (cold losses). The pressure drops due to the heat addiction (hot losses) are far less significant than the previous contribution [44]. Hence, Eq. (14) has been employed [43].

$$\frac{\frac{\Delta P_{3-4}}{P_3}}{\left(\frac{\Delta P_{3-4}}{P_3}\right)_{des}} = \left[\frac{\frac{\dot{m}_3\sqrt{RT_{03}}}{P_{03}}}{\left(\frac{\dot{m}_3\sqrt{RT_{03}}}{P_{03}}\right)_{des}}\right]^2 \tag{14}$$

D. Weight Model

A detailed weight model has been created using information provided in [45, 46] for the following components: compressors, combustor, turbines, shaft and accessories. The geometrical data necessary for the model has been derived from the preliminary component design technique discussed previously.

Since it is common to specifically design heat exchangers for the given case of study [3, 47, 48], a detailed intercooler/recuperator geometrical characterization cannot be obtained at preliminary design stages. Therefore, the heat exchangers weight has been estimated by means of relations provided in [10, 49–51]. These relate cycle flow parameters (overall pressure ratio, inlet mass flow, etc.) to intercooler and recuperator volumes, in a similar fashion to Eq. (1).

The propeller gearbox weight has been calculated using the methodology discussed in reference [52] and assuming a planetary gearbox. The propeller weight contribution has not been accounted for since the propeller has only been treated as a load and a detailed geometrical model has not been defined. Equation (15) is used to calculate the overall engine weight.

$$W_{eng} = W_C + W_{IC} + W_{RC} + W_B + W_T + W_{sh} + W_{gear} + W_{acc} \tag{15}$$

While only moderate accuracy can be expected with the implemented component weight model due to the lack of well documented open source references. Therefore the scope of this model is to characterize the component size variation as function of thermodynamic inputs, such that the optimizer can perform the trade-offs between weight and specific fuel consumption adequately. For the case studies reported here the trends in weight are thus more important than the absolute values.

More details are provided below for weight estimation of compressor, turbine and heat exchangers. More information on the whole weight assessment procedure can be found in [5].

1. Compressor Weight

The compressor overall weight is split into the contribution of blades, disk, shroud and diffuser [45]. The first contribution is computed assuming that the flow path is comprised between two ellipses, while defining the hub and tip blade thickness from statistical data reported in [53]. Once the blade volume is available the weight is computed by multiplying it by the density of the chosen material.

Since insufficient information is available in [45, 46] to calculate the disk weight, a procedure has been derived in [5] to preliminary assess this contribution. The resulting model has been calibrated using Eq. (16) [46], valid only for titanium alloys, and compressor statistical weight data given in [53].

$$W_C = \frac{1}{13.1} \cdot r_2^3 \tag{16}$$

Finally, the shroud and diffuser weight contributions have been calculated using Eqs. (17) and (18) respectively [45]:

$$W_{shroud} = 0.1673\rho \left(\frac{r_{1s} + r_2}{2} \right)^3 \tag{17}$$

and

$$W_{diffuser} = 0.2845\rho r_2^3 \tag{18}$$

A compressor material database has been created from [54] which is used to define the material density needed for the weight calculations. A preliminary blade and disk stress assessment is made during the weight calculation to establish whether the selected material can cope with the centrifugal stresses. Equations (19) [55] and (20) [54] have been used for disk and blade stress calculations respectively.

$$\sigma_{disk} = \frac{K_{disk}}{3} \rho \omega^2 r_2^2 \tag{19}$$

and

$$\sigma_{blade} = \frac{\rho \omega^2 r_2 b_2^2}{t_{hub}^2} (t_{hub} + 2t_{tip}) \sin \beta_2 \tag{20}$$

where the constant K_{disk} has been conservatively set to 3.0, as explained in [5]. The titanium alloy Ti-6Al-4V is initially assumed. If the given rotational speed leads to unfeasible disk or blade stresses, a different material will be tried

until a feasible solution has been found or all materials have failed the test. In this last event, the optimizer proceeds to discard the design vector combination as it is an unfeasible design.

In addition, reference [46] provides Eq. 21 to calculate the compressor case weight. Note that the dimensions used for this equation must be defined in British units. The same material as that employed for impeller and diffuser has been assumed here.

$$W_{case} = 163 \cdot L_{ax} \cdot r_2 \tag{21}$$

2. Turbine Weight

The turbine weight has been obtained using a similar approach to that adopted for the compressor. The blade and disk weight contribution has been identically calculated, while for the shroud Eq. (22) has been used [45].

$$W_{shroud} = 0.1755\rho \left(\frac{r_{3s} + r_2}{2} \right)^3 \tag{22}$$

The model has been calibrated using the simplified turbine relation given in ref. [46] which is valid for a steel based alloy (Eq. 23). This was done to ensure that a more consistent weight trend was obtained in comparison with the available reference data. Because of the uneven temperature and stress distribution, Eqs. (19) and (20) cannot be reliably employed in determining the maximum turbine stress levels [54, 55]. Therefore, the turbine material is selected purely based on the TIT, among the material database created of nickel and cobalt based alloys [54].

Reference [46] suggests to employ Eq. (23) to calculate the turbine rear frame weight. This contribution has been added to the model.

$$W_{frame} = 55.5 \cdot r_2^2 + 6.53 \tag{23}$$

3. Heat Exchangers Weight

Reference [51] uses Eq. (1) to develop a preliminary approach which allows to estimate the recuperator weight from given reference data. The surface geometry part of the equation is not considered and the weight is assumed to be function only of the heat exchanger performance characteristics. A similar approach has been discussed in [49, 50], leading to the definition of Eq. (24),

$$W_{RC} = W_{ref} \cdot \left\{ \left[\frac{\dot{m}}{\sqrt{\Pi_C}} \left(\frac{\varepsilon}{1-\varepsilon} \frac{1}{\sqrt{\Delta P/P}} \right) \right] / \left[\frac{\dot{m}_{ref}}{\sqrt{\Pi_{C,ref}}} \left(\frac{\varepsilon_{ref}}{1-\varepsilon_{ref}} \frac{1}{\sqrt{(\Delta P/P)_{ref}}} \right) \right] \right\} \tag{24}$$

A similar relation can be derived for the intercooler (Eq. 25) [10, 50] where the dependency on the cycle pressure ratio has been substituted by the arithmetic mean between the inlet hot and cold side pressures.

$$W_{IC} = W_{ref} \cdot \left\{ \left[\frac{\dot{m}}{\sqrt{P_{mean}}} \left(\frac{\varepsilon}{1-\varepsilon} \frac{1}{\sqrt{\Delta P/P}} \right) \right] / \left[\frac{\dot{m}_{ref}}{\sqrt{P_{mean,ref}}} \left(\frac{\varepsilon_{ref}}{1-\varepsilon_{ref}} \frac{1}{\sqrt{(\Delta P/P)_{ref}}} \right) \right] \right\} \tag{25}$$

Recuperator and intercooler reference data have been taken from [50], allowing for the preliminary component weight estimation. Validation of this model has been made with real heat exchanger weight data available in [47, 56], showing good agreement with conventional heat exchanger configurations (tube and plate fin).

E. Multi-Objective Optimization

The developed model has been coupled with an external optimizer to perform the multi-objective optimization and trade-off between engine weight and part-power specific fuel consumption (SFC). The mathematical description of problem is summarized in Eq. (26). No direct constraints have been applied to the optimizer, since feasibility of the designs has been already ensured inside NPSS and the various component models. However, bounds have been set for the various input parameters to define the algorithm searching path, depending on the engine under investigation.

$$min[\bar{J}(x)] = min \begin{bmatrix} J_1(x) \\ J_2(x) \end{bmatrix} = min \begin{bmatrix} SFC_{av}(x) \\ W_{eng}(x) \end{bmatrix} \tag{26}$$

subjected to

$$x_l \leq x \leq x_u$$

Where SFC_{av} has been defined as the average between the design specific fuel consumption, assumed at 100% of the propeller power demand and the part power SFC values calculated at 75%, 50%, and 25% of the design power:

$$SFC_{av} = \frac{SFC_{des} + SFC_{75\%} + SFC_{50\%} + SFC_{25\%}}{4} \tag{27}$$

Part-power SFC is used to ensure that the optimizer does not exploit a design point with lower fuel consumption at the expense of a sharp increase in SFC at part-power.

The optimization has been set up in Matlab using the in-built multi-objective evolutionary algorithm "gamultiobj". This algorithm has been used for the coupling with the developed modeling environment, since it allows for a much greater exploration of the whole design space than gradient based optimizers. Figure 5 summarizes the model integration with the optimizer.

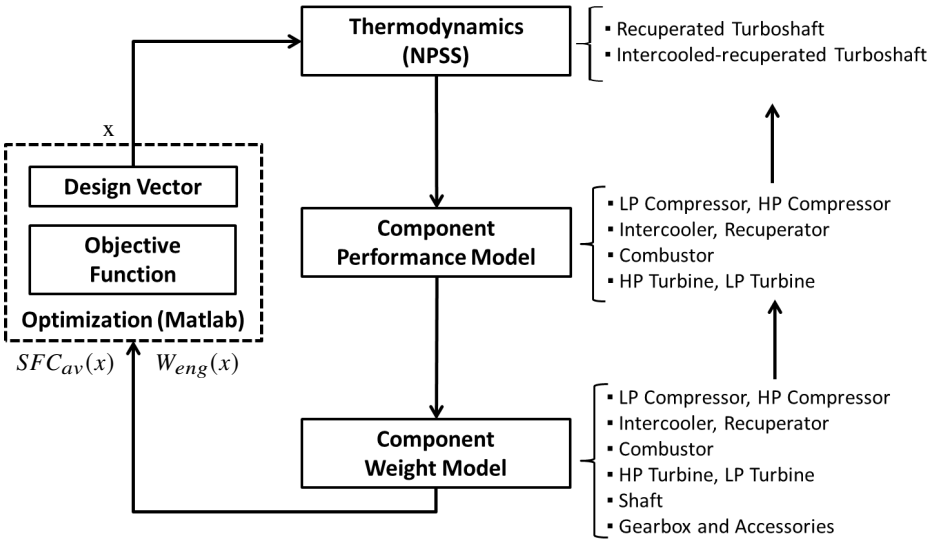

Fig. 5 Optimization modeling diagram

"gamultiobj" generates a new design vector at each iteration that is used to run the thermodynamic analysis in NPSS. Thermodynamic output data from NPSS are then used to run the component performance model which updates component efficiencies, defines the geometry, and calculates the engine weight. Several iterations are needed between the performance module and NPSS such that component efficiencies are properly updated based on the input parameters. Finally, the objective function can be determined and the Matlab algorithm can continue.

The design vector includes primary cycle thermodynamic variables as well as important turbomachinery parameters. Thermodynamic design variables used for the case studies reported here are given in Table 4. They mainly consist of the compressor pressure ratios and heat exchanger effectiveness and pressure drops. As mentioned earlier the heat input into the intercooler is set to zero for the simple recuperated engine configuration, and the corresponding input variables are thus removed from the design vector.

In addition to the thermodynamic design parameters, turbomachinery input parameters are modified by the optimizer to obtain maximum efficiency or minimum size, while ensuring machine feasibility. Table 5 shows the compressor design variables and relative bounds used for the optimization. References are provided to support the selection of the various upper and lower bounds. Table 6 details the design vector used for the turbine element with related references.

Table 4 Thermodynamic design variables and relative bounds

x	x_l	x_u	Reference
Π_{LPC}	2.000	5.000	-
Π_{HPC}	3.000	6.000	-
$(\Delta P/P)_{IC,h}$	0.020	0.050	-
ε_{IC}	0.650	0.950	-
$(\Delta P/P)_{RC,c}$	0.020	0.050	[47, 56, 57]
$(\Delta P/P)_{RC,h}$	0.020	0.050	[47, 56, 57]
ε_{RC}	0.650	0.950	[56, 57]
TIT	1200K	1650K	[57]
$\%P_{04,LPC}$	0.850	1.150	-
Π_{Noz}	1.050	1.250	[58]
N	8500	13500	-

Table 5 Compressor design variables and relative bounds

x	x_l	x_u	Reference
ν	0.300	0.700	[14, 16, 59, 60]
α_2	60°	70°	[14, 15]
β_2	-40°	0°	[14, 15]
$2\theta_c$	7°	11°	[20]

The low pressure compressor (LPC) exit Mach number has been added as an additional design variable to ensure the most optimal matching with the following element in the cycle.

Table 6 Turbine design variables and relative bounds

x	x_l	x_u	Reference
r_0/r_1	1.100	1.700	[61]
ν	0.300	0.700	[30, 62]
β_{3s}	-70°	-50°	[14, 29]

Performance of evolutionary algorithms can be strongly influenced by the population size, especially for problems with a high dimension in the design vector. Here, the initial population size has been determined with the general rule of thumb reported in [63]. The population size is set to ten times the number of design variables which ensures that a smooth Pareto frontier is obtained for the case studies reported here. The default "gamultiobj" stopping criteria have been left unaltered, which led to convergence in approximately 110 generations for each engine model.

IV. Case Studies

The presented design and optimization tool has been used in two case studies, whose main design operating conditions have been summarized in Table 7. For each case study, the simple recuperated and the intercooled-recuperated gas turbine configuration have been investigated. Each engine architecture constitutes of a set of two centrifugal compressors, powered by two radial turbines, and connected by means of a single shaft. The propeller is linked to the gas turbine with a reduction gearbox.

As a single shaft architecture has been selected, an additional condition on the power split between the two turbines is provided to NPSS to complete the cycle analysis. This has been implemented by defining the HPT exit pressure ratio

as a certain percentage of the LPC exit pressure. The optimizer acts on this percentage to establish the most optimal power split for minimum weight or minimum SFC.

Table 7 Engine main design characteristics

	Alt (ft)	M_{flight}	$\dot{W}_{des}$ (hp)
Case 1	90000	0.4	300
Case 2	20000	0.4	100

A discussion of the case studies is reported next, showing specific thermodynamic design variables settings and bounds used for each engine analysis. Furthermore, the outcome of the optimization is presented, highlighting the benefit of the implemented optimization tool.

A. Case 1

The optimization results for the simple recuperated and the intercooled-recuperated engines are provided below for those thermodynamic variables that have a significant effect on the engine performance and weight. Results have been presented by displaying the Pareto frontier on multiple variables 2D scatter plots. For each plot one input parameter is represented by the color of the scatter bubble, while the radius of the bubble indicates the value of the second input parameter. This allows to highlight the influence of primary engine design variables on the two objectives, helping the selection of preliminary engine design variables for further detailed evaluations. Results of both RC and ICR engines are presented side by side to enable comparison between the two engine types.

1. Effects of OPR and RPM

Figure 6 shows the impact of overall pressure ratio and rotational speed on the weight and SFC for both recuperated and intercooled-recuperated gas turbines. An increase in OPR leads to a reduction of the required inlet mass flow. Hence the optimizer increases OPR until a further pressure rise will offset the recuperator performance or the engine feasibility is compromised. For the recuperated engine the optimum OPR remains fairly constant across the entire Pareto frontier. For the ICR a larger variation in OPR is found across the frontier. Lower OPR values result in lighter engines while slightly higher values can be adopted for minimum SFC. Minimum fuel consumption for the ICR is slightly lower than that of the simple recuperated engine and occurs at an OPR around 16. For the simple recuperated engine the OPR that leads to minimum SFC is around 13.

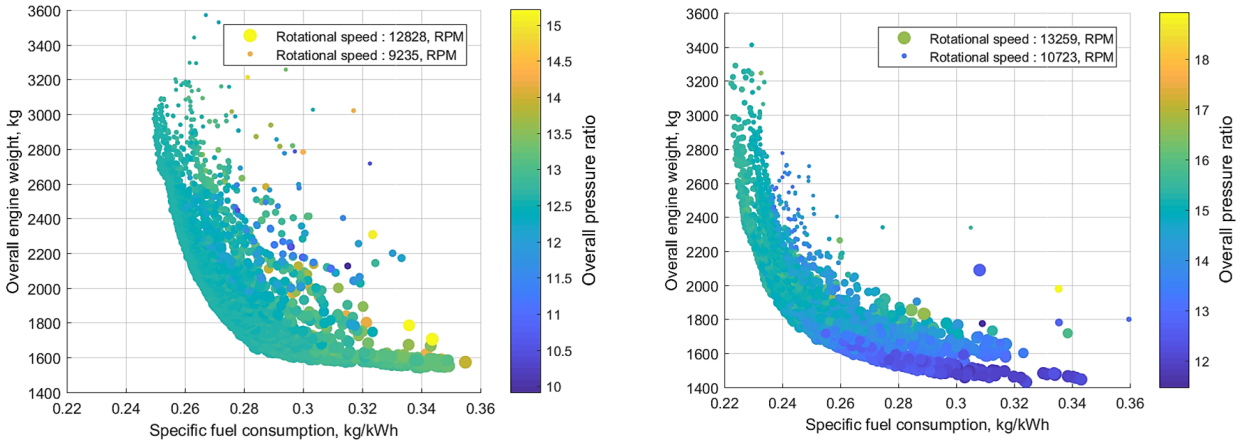

(a) Simple recuperated engine

(b) Intercooled-recuperated engine

Fig. 6 Effect of overall pressure ratio and rotational speed

The benefits of higher rotational speeds for minimum weight is clearly visible from figure 6, since a considerable turbomachinery weight reduction becomes possible. On the other hand, for minimum SFC solutions, almost the same pressure rise is obtained through a slightly larger turbomachinery block. In fact, lower efficiency penalties, due to

secondary and shock losses, are registered by the model for reduced rotational speeds, thus improving the overall thermal efficiency of the engine at the expense of an increase in engine weight.

Despite the addition of the intercooler engine weights are similar for both cycles. This suggests that the higher specific power of the intercooled-recuperated engine cycle offsets the weight of the additional heat exchanger.

2. Effects of TIT

Increasing the turbine inlet temperature is advantageous for both objectives, as a high TIT improves the engine thermal efficiency and specific power simultaneously. The main limitation on the maximum TIT is thus primarily given by the technological level of turbine, combustor and recuperator materials. Since the first two aspects are considered within the component models and the selected bounds, an external variable is passed to NPSS to define the maximum admissible recuperator inlet temperature (RIT). The optimizer automatically deals with unfeasible recuperator inlet flows, discarding the point at the next generation.

In this example, a maximum RIT value of 900°C (1173.15K) has been set, which represents the maximum limit for metallic alloys [3]. Figure 7 summarizes the optimization output for the TIT design variable. As shown the optimal TIT for the recuperated engine is around 1520 K. The addition of the intercooler allows a slight increase in TIT with values up to 1570 K. A higher TIT can be reached without exceeding the recuperator material limit as the higher OPR of the ICR engine leads to a more substantial expansion in the high pressure turbine.

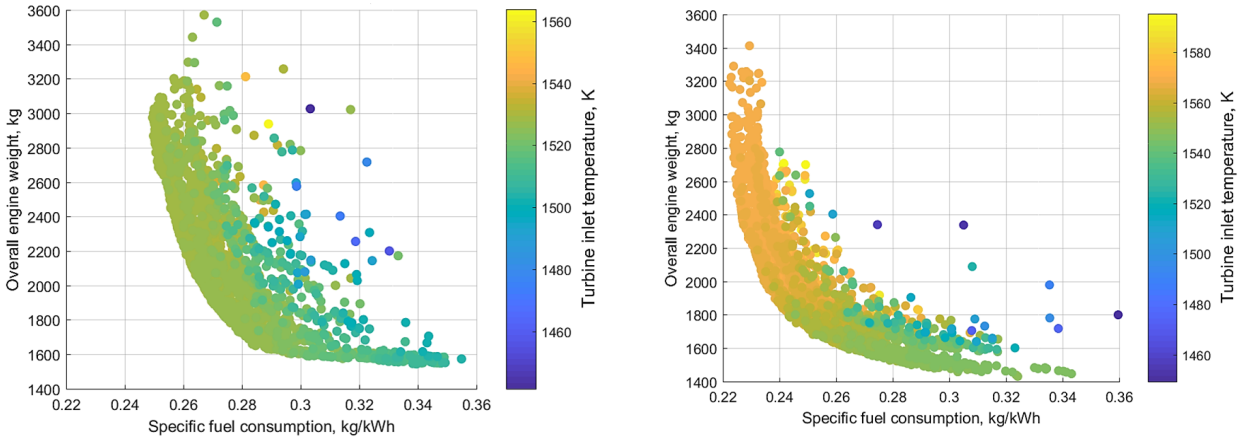

(a) Simple recuperated engine

(b) Intercooled-recuperated engine

Fig. 7 Effect of turbine inlet temperature

3. Effects of HEXs

Effects of intercooler hot side pressure drops and effectiveness are given in Fig. 8 for the ICR engine. As shown, the substantial influence of intercooler effectiveness and hot side pressure loss on cycle performance and weight is captured well by the analysis. In fact, high effectiveness and low pressure drop are typical of minimum SFC solutions, vice versa for minimum weight.

Similar considerations are applicable to the recuperator, as visible from Fig. 9. The optimizer maximizes the recuperator effectiveness and minimizes the total pressure losses (given as sum of hot and cold side losses) for minimum SFC solutions and vice versa for minimum weight. By looking at the NPSS raw data, it becomes evident how the hot side pressure drop has a much stronger impact on engine performance than the cold side pressure drop. Therefore, this contribution is often minimized to reduce the SFC, confirming the detailed considerations reported in [4].

Heat exchanger considerations give evidence of the advantages of the developed engine optimization tool. In fact, with the current model, the strong integration between cycle thermodynamics and component performance is much better captured. For example, the heat exchangers upper and lower bounds are not reached for minimum weight or SFC solutions. Instead, the advantages that better HEX performance would introduce are weighed by the optimizer against the effects that the resultant cycle flow conditions have on other components.

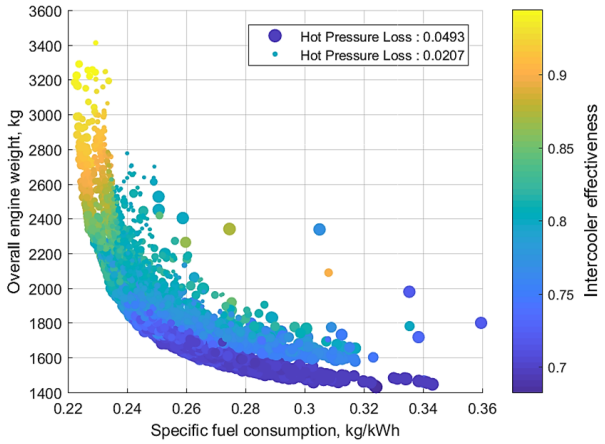

Fig. 8 Effects of intercooler parameters

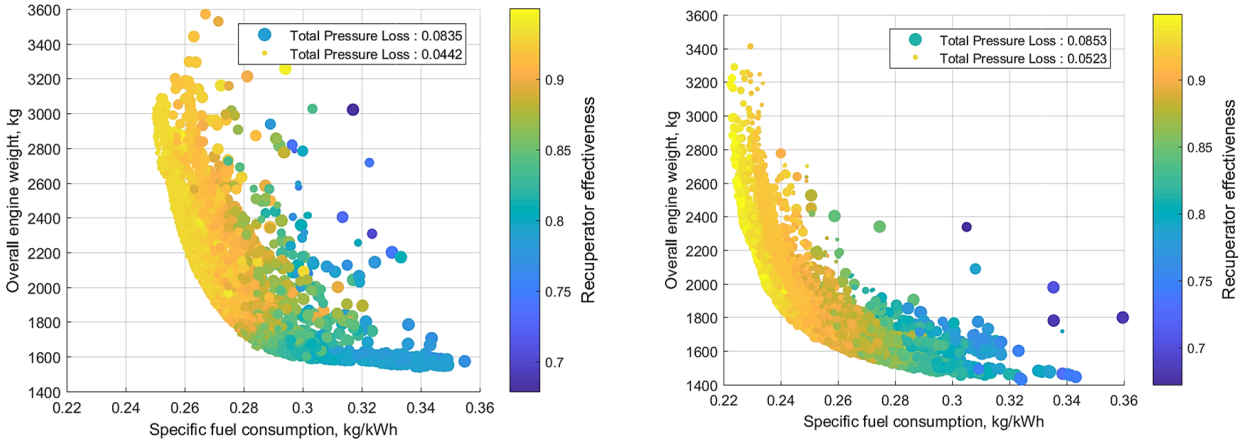

(a) Simple recuperated engine

(b) Intercooled-recuperated engine

Fig. 9 Effect of recuperator parameters

4. Effects of Power Split and Nozzle Pressure Ratio

The effect of turbine power split and nozzle pressure ratio on the objectives are documented in Fig. 10. Similar considerations can be made for the power split in both RC and ICR engines. In particular, the engine is balanced such that most of the power is extracted from the HPT, which allows for a higher turbine inlet temperature for a given recuperator material limit. However, the optimal power split is set to avoid an excessive enthalpy drop and a corresponding low recuperator inlet temperature so that a sufficient temperature difference is achieved across the recuperator for a good heat transfer.

A similar behavior is also apparent for the nozzle pressure ratio variable between the two engine arrangements. Since the nozzle design pressure ratio directly affects the engine overall inlet mass flow, a low value of this variable contributes to minimize both objectives. However, because the optimization has to account for part power behavior as well, the design nozzle pressure drop is picked to ensure satisfactory cycle off-design performance. After all, the nozzle pressure ratio reduces at part power. Hence, minimum weight solutions have a slightly higher Π_{Noz} value.

5. Effects of Turbomachinery Geometry

The compressors and turbines geometrical parameters given in tables 5 and 6 have a much less impact on the overall cycle than the previously discussed variables. Their influence is mainly related to individual turbomachinery efficiency and feasibility. Hence, the optimizer similarly selects these variables for both objectives to ensure that maximum efficiency or minimum size is achieved for the given flow condition. More information on the selected values for these

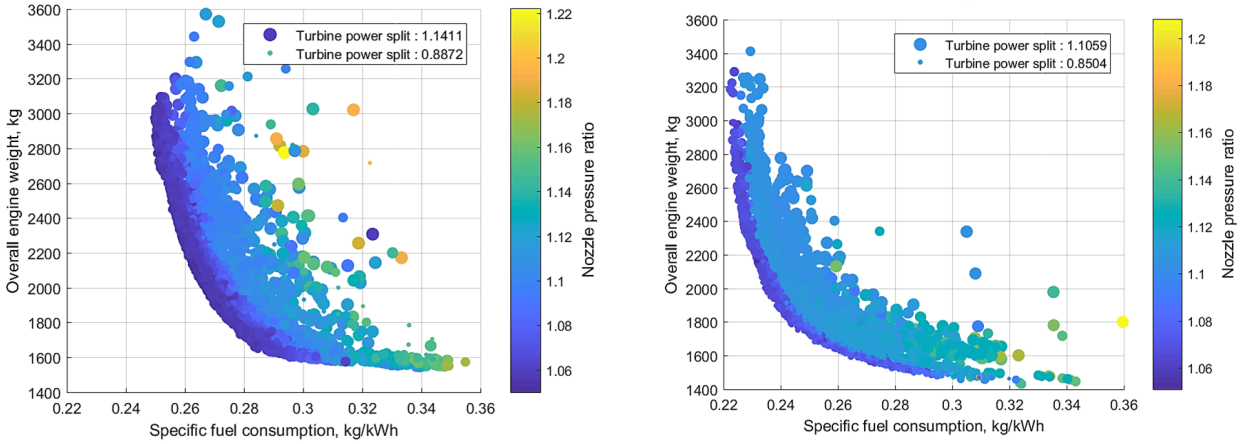

(a) Simple recuperated engine

(b) Intercooled-recuperated engine

Fig. 10 Effect of turbine power split and nozzle pressure ratio

design vectors is available in [5].

B. Case 2

For the second case study the same engine configurations are considered albeit at a much lower altitude and smaller engine size. To account for this smaller engine size, the upper and lower bounds for the rotation speed have been changed, as shown in Table 8. These modifications have been made after a preliminary feasibility study was performed with the model. All other bounds remain unaltered from the previous case study.

Table 8 Modified rotational speed bounds

Engine	x_l	x_u
RC	50000	100000
ICR	60000	120000

A similar set of results has been obtained for the second case study. However, lower design altitude and small engine size have a much greater impact on the overall performance of the simple recuperated and the intercooled-recuperated engines. The resultant Pareto frontier is reported below, showing the influence of major design variables on the optimization objectives. A brief explanation is given for trends that strongly differ from the previous example.

1. Effects of OPR and RPM

As shown in Fig. 11 the optimal overall pressure ratio is much more constrained by the recuperator performance than for the previous case. The relatively low optimal OPR output values of the simple recuperated engine seem not to justify a double compressor arrangement, which leads to a quite significant overall engine weight, due to turbomachinery size. On the other hand, the intercooled-recuperated engine has its optimum at higher overall pressure ratio, which is achievable due to the intercooler presence. However, since a much lower mass flow rate is needed for the same power output, with respect to the RC engine, a smaller turbomachinery block is needed. This aspect strongly limits the maximum efficiency achievable from compressors and turbines, thus leading to an overall cycle performance which is comparable with the simple recuperated gas turbine. Rotational speed considerations remain unchanged with respect to the previous case of study.

2. Effects of TIT

The turbine inlet temperature effects on the overall thermal efficiency and engine weight are in agreement with what previously discussed. However, the RC engine runs with a much lower TIT than the high altitude case study, due to the imposed limitation on the RIT, and the low pressure ratios achieved by the cycle. For the ICR cycle similar TIT values are obtained for both case studies.

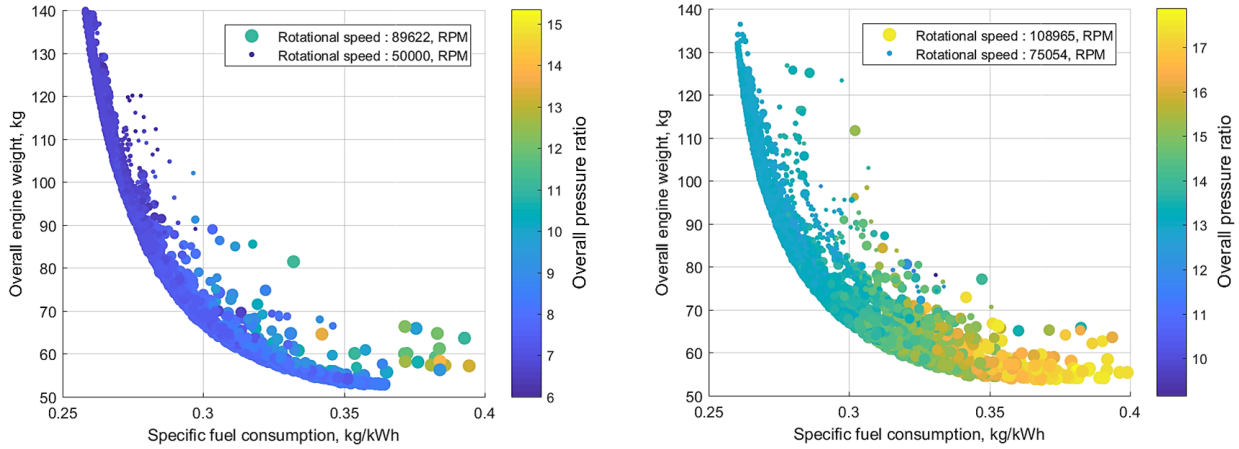

(a) Simple recuperated engine **(b) Intercooled-recuperated engine**

Fig. 11 Effect of overall pressure ratio and rotational speed

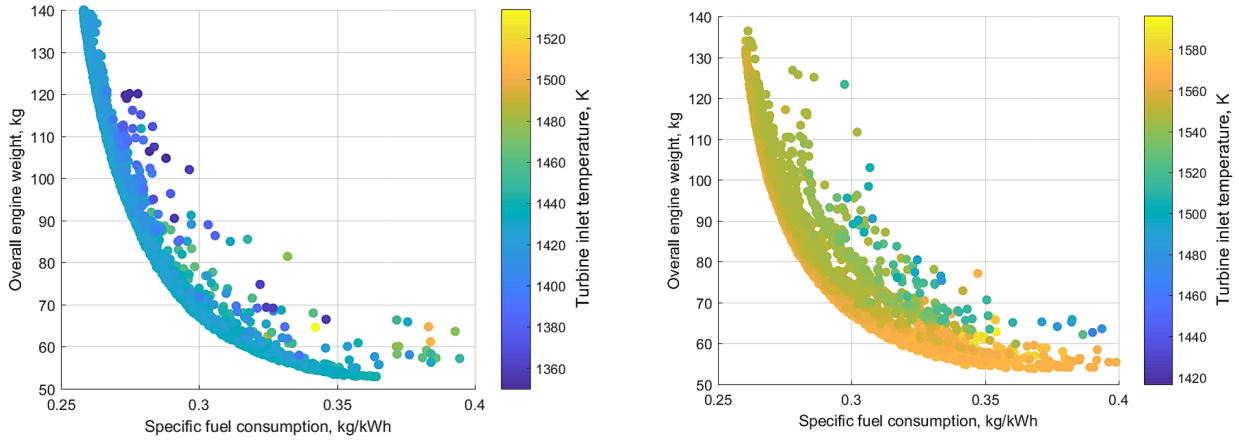

(a) Simple recuperated engine **(b) Intercooled-recuperated engine**

Fig. 12 Effect of turbine inlet temperature

3. Effects of HEXs

Although the trend is still maintained, the intercooler maximum effectiveness becomes slightly less important for the minimum SFC solutions in comparison to the previous case study. This can been explained by considering the turbomachinery efficiency variation as function of the intercooler effectiveness. In particular, for the same power output and TIT, an increase of ε_{IC} causes a reduction of the engine mass flow rate, which reduces the overall turbomachinery size and results in a lower efficiency for the turbomachinery components [64, 65].

Because the recuperator has a comparatively higher impact on the overall cycle performance, the optimizer establishes the overall cycle optimum at a lower intercooler effectiveness, allowing for greater recuperator heat transfer. Figures 13 and 14 (b) give evidence of these trends.

4. Effects of Power Split and and Nozzle Pressure Ratio

Figure 15 shows the effects of power split and nozzle pressure ratio on the optimization objectives. Similar observations to the 300hp case study can be derived here for the first parameter. In fact, most of the turbine power is again extracted from the HPT for both simple recuperated and intercooled-recuperated engines, due to the same reasons previously given. A higher HPT expansion namely enables a higher TIT without reaching the recuperator material limit.

Agreement with the 300hp trend has been also maintained for the nozzle pressure ratio, where a slightly higher

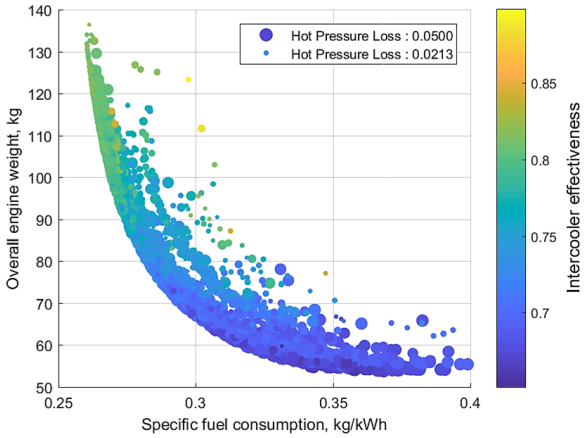

Fig. 13 Effects of intercooler parameters

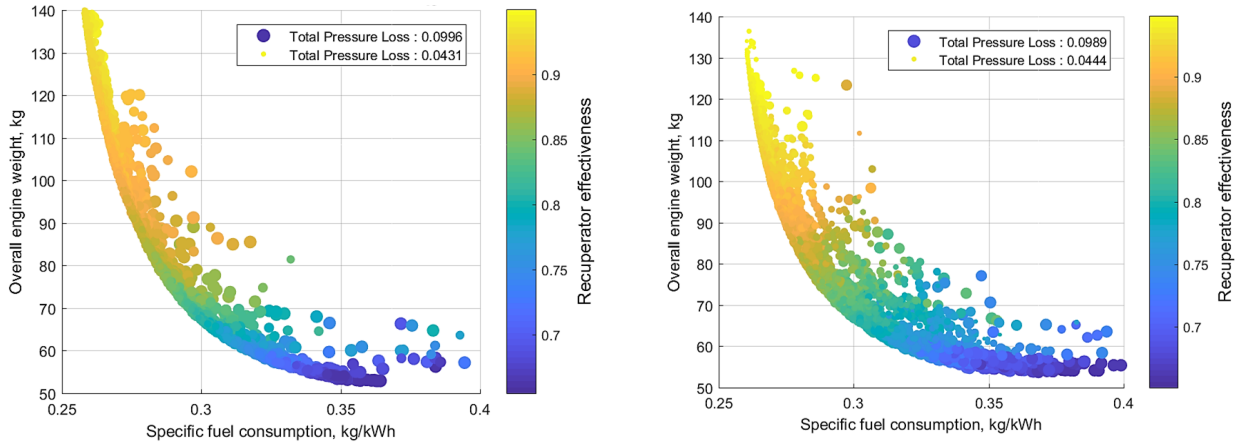

(a) Simple recuperated engine

(b) Intercooled-recuperated engine

Fig. 14 Effect of recuperator parameters

value has been obtained for minimum weight. However, because the engine is designed for a more conventional altitude, the off-design flow conditions has a smaller impact on the optimum nozzle pressure ratio, leading to a lower difference of Π_{Noz} between minimum SFC and weight solutions (Fig. 15).

V. Conclusion

An advanced methodology has been implemented for the preliminary design study of a simple recuperated and intercooled-recuperated gas turbine. The purely thermodynamic study has been supported by a component based approach which accurately predicts the variation of performance and size as function of overall cycle parameters.

The tool has been coupled with an evolutionary algorithm to optimize the cycle design point considering part power performance at the operating design condition. Since engine feasibility is ensured by the component model, the optimizer produces a set of Pareto optimal solutions that can be employed to select engine design features for the given application much more accurately than conventional approaches that are typically used in early design stages.

Examples have been given with a single shaft architecture for an unconventional high altitude and a medium altitude recuperated and intercooled-recuperated UAV gas turbines. Altitude and size effects are well captured by the turbomachinery model, making the optimization much more sensitive to the variation of flow characteristics due to thermodynamic modification.

Since the tool can be customized to define new cycle configurations in NPSS, a set of different design and component arrangements can be quickly assessed. Thus, promptly identifying limitations in the selected architecture and facilitating

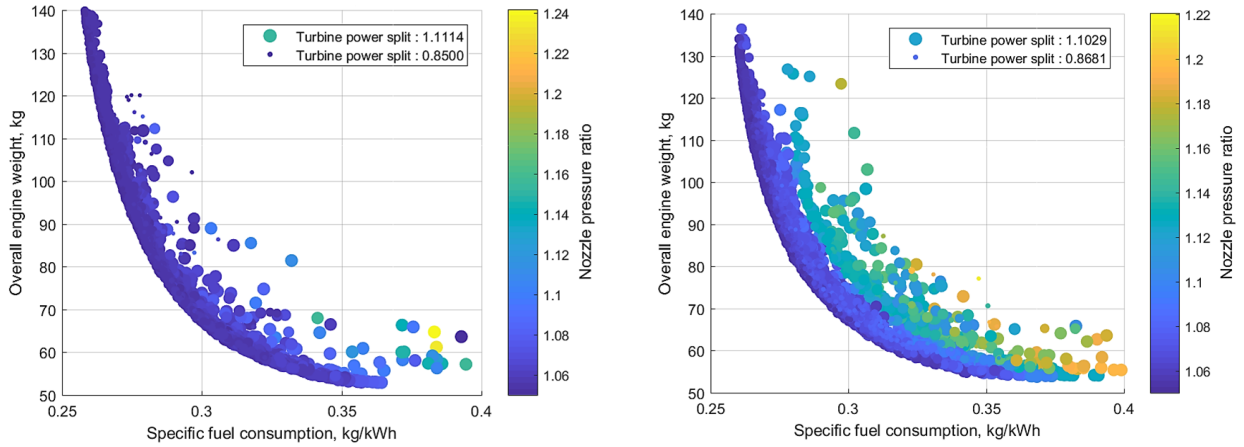

(a) Simple recuperated engine

(b) Intercooled-recuperated engine

Fig. 15 Effect of turbine power split and nozzle pressure ratio

the preliminary design identification for future more detailed considerations.

References

[1] McDonald, C. F., "Heat Recovery Exchangers Technology for Very Small Gas Turbines," *International Journal of Turbo and Jet Engines*, Vol. 13, No. 4, 1996, pp. 239–261.

[2] McDonald, C. F., "Low-cost compact primary surface recuperator concept for microturbines," *Applied Thermal Engineering*, Vol. 20, No. 5, 2000, pp. 471–497.

[3] McDonald, C. F., "Recuperator considerations for future higher efficiency microturbines," *Applied Thermal Engineering*, Vol. 23, 2003, pp. 1463–1487.

[4] Stevens, T., Verplaetsen, F., and Baelmans, M., "Requirements for recuperators in micro gas turbines," *International workshop on micro and nanotechnlogy for power generation and energy conservation application*, Kyoto, Japan, 2004, pp. 96–99.

[5] Tacconi, J., "Investigation of a semi-closed cycle small gas turbine for high altitude UAV propulsion," , 2018. Unpublished.

[6] Jones, S. M., "An Introduction to Thermodynamic Performance Analysis of Aircraft Gas Turbine Engine Cycles Using the Numerical Propulsion System Simulation Code," Tech. rep., NASA Glenn Research Center, Cleveland, Ohio, USA, 2007.

[7] Kumar, G. N., and DeAnna, R. G., "Development of a Thermal and Structural Analysis Procedure for Cooled Radial Turbines," *33rd International Gas Turbine and Aeroengine Congress and Exposition*, ASME, Amsterdam, The Netherlands, 1988.

[8] Snyder, P. H., "Cooled High-Temperature Radial Turbine Program," Tech. rep., Allison Gas Turbine Division General Motors Corporation, 1992.

[9] Lane, J. M., "Cooled Radial In-Flow Turbines for Advanced Gas Turbine Engines," *Gas Turbine Conference & Products Show*, ASME, Houston, Texas, USA, 1981, pp. 1–9.

[10] Rodgers, C., "A Cycle Analysis Technique for Small Gas Turbines," *Proceedings of the Institution of Mechanical Engineers*, Vol. 183, 1969, pp. 37–49.

[11] Horlock, J. H., Watson, D. T., and Jones, T. V., "Limitations on Gas Turbine Performance Imposed by Large Turbine Cooling Flows," *Journal of Engineering for Gas Turbines and Power*, Vol. 123, No. 3, 2001, p. 487.

[12] Kurzke, J., "Achieving maximum thermal efficiency with the simple gas turbine cycle," Tech. rep., MTU Aero Engines, 2018.

[13] Kurzke, J., "Aero-Engine Design: A State of the Art," , 2003.

[14] Whitfield, A., and Baines, N., *Design of Radial Turbomachines*, Pearson Education, 1990.

[15] Whitfield, A., "Preliminary Design and Performance Prediction Techniques for Centrifugal Compressors," *Proceedings of the Institution of Mechanical Engineers*, Vol. 204, No. 1, 1990, pp. 131–144.

[16] Galvas, M. R., "Analytical Correlation of Centrifugal Compressor Design Geometry for Maximum Efficiency with Specific Speed," Tech. rep., NASA Lewis Research Center, Cleveland, Ohio, USA, 1972.

[17] Kim, Y., Engeda, A., Aungier, R., and Amineni, N., "A centrifugal compressor stage with wide ow range vaned diffusers and different inlet con gurations," *Journal Power and Energy*, Vol. 216, 2002, pp. 307–320.

[18] Galvas, M. R., "Fortran Program for Predicting Off-Design Performance of Centrifugal Compressors," Tech. rep., NASA Lewis Research Center and U.S. Army Air Mobility R&D Laboratory, Cleveland, Ohio, USA, 1973.

[19] Oh, H. W., Yoon, E. S., and Chung, M. K., "An optimum set of loss models for performance prediction of centrifugal compressors," *Proceedings of the Institution of Mechanical Engineers, Part A: Journal of Power and Energy*, Vol. 211, No. 4, 1997, pp. 331–338.

[20] Aungier, R. H., *Centrifugal Compressors A Strategy for Aerodynamic Design and Analysis*, ASME, 2000.

[21] Aungier, R. H., "Mean Streamline Aerodynamic Performance Analysis of Centrifugal Compressors," Vol. 117, 1995, pp. 360–366.

[22] Harley, P., Spence, S., Early, J., Filsinger, D., and Dietrich, M., "An evaluation of 1D loss model collections for the off-design performance prediction of automotive turbocharger compressors," *6th International Conference on Pumps and Fans with Compressors and Wind Turbines*, IOP, 2013.

[23] Rodgers, C., "Impeller Stalling as Influenced by Diffusion Limitations," *Journal of Fluids Engineering*, 1977, pp. 84–93.

[24] Japikse, D., and Baines, N., *Introduction to Turbomachinery*, 1997.

[25] Heidelberg, L. J., Bull, C. L., and Weigel, C., "Effect Of Reynolds Number on Overall Performance of a 6-inch Radial Bladed Centrifugal Compressor," Tech. rep., NASA Lewis Research Center, Cleveland, Ohio, USA, 1970.

[26] Klassen, H. A., Wood, J. R., and Schummann, L. F., "Experimental Performance of a 16.10-Centimeter-Tip-Diameter Sweptback Centrifugal Compressor Designed for a 6:1 Pressure Ratio," Tech. rep., NASA Lewis Research Center and U.S. Army Air Mobility R&D Laboratory, Cleveland, Ohio, USA, 1977.

[27] Eisenlohr, G., Krain, H., Richter, F.-A., and Tiede, V., "Investigations of the Flow Through a High Pressure Ratio Centrifugal Impeller," *ASME Turbo Expo*, ASME, Amsterdam, The Netherlands, 2002, pp. 1–9.

[28] Yoshinaka, T., Thompson, R. G., and Letourneau, J., "The Performance Prediction and Demonstration of a Centrifugal Compressor for the Multiple Purpose Small Power Unit (MPSPU)," *Gas Turbine and Aeroengine Congress and Exposition*, ASME, Totonto, Ontario, Canada, 1989.

[29] Whitfield, A., "The Preliminary Design of Radial Inflow Turbines," *Journal of Turbomachinery*, Vol. 112, No. 1, 1989, pp. 50–57.

[30] Rohlik, H. E., "Analytical Determination of Radial Inflow Turbines Design Geometry for Maximum Efficiency," Tech. rep., NASA Lewis Research Center, Cleveland, Ohio, USA, 1968.

[31] Glassman, A. J., *Turbine Design and Application (3 volumes)*, National Aeronautical and Space Administration, Washington D.C., USA, 1973.

[32] Glassman, A. J., "Computer Program for Design Analysis of Radial-Inflow Turbines," Tech. rep., NASA Lewis Research Center, Cleveland, Ohio, USA, 1976.

[33] Wasserbauer, C. A., and Glassman, A. J., "Fortran program for predicting off-design performance of radial-inflow turbines," Tech. rep., NASA Lewis Resedrcb Center, Cleveland, Ohio, USA, 1975.

[34] Baines, N., "A meanline prediction method for radial turbine efficiency," *Sixth International Conference on Turbocharging and Air Management Systems*, Vol. 1998, 1998, pp. 45–56.

[35] Khader, M., "Optimised Radial Turbine Design D1.8," , 2014.

[36] Ventura, C. A. M., Jacobs, P. A., Rowlands, A. S., Petrie-repar, P., and Sauret, E., "Preliminary Design and Performance Estimation of Radial Inflow Turbines : An Automated Approach," Vol. 134, 2012, pp. 1–13.

[37] McLallin, K. L., and Haas, J. E., "Experimental Performance and Analysis of 15.04-Centimeter-Tip-Diameter, Radial-Inflow Turbine with Work Factor of 1.126 and Thick Blading," Tech. rep., NASA Lewis Research Center, Cleveland, Ohio, USA, 1980.

[38] Pullen, K. R., Baines, N. C., and Hill, S. H., "The Design and Evaluation of a High Pressure Ratio Radial Turbine," *International Gas Turbine & Aeroengine Congress & Exhibition*, ASME, Cologne, Germany, 1992, pp. 1–7.

[39] Melconian, J. O., and Modak, A. T., "Combustor Design, in Sawyer's gas turbine engineering handbook," *Turbomachinery International Publications*, Vol. 1, 1985.

[40] Kowaiski, E. J., and Atkins, R. A., "A Computer Code for Estimating Installed Performance of Aircraft Gas Turbine Engines," Tech. rep., Advanced Airplane Branch Boeing Military Airplane Company, Seattle, Washington, USA, 1979.

[41] Schutte, J. S., "Simultaneous Multi-Design Point Approach to Gas Turbine On-Design Cycle Analysis for Aircraft Engines," Ph.D. thesis, Georgia Institute of Technology, 2009.

[42] Walsh, P. P., and Fletcher, P., *Gas Turbine Performance*, 2nd ed., Blackwell, 2004.

[43] Zafer, L., "An investigation into performance modeling of a small gas turbine engine," Tech. rep., Australian Government Department of Defence, 2012.

[44] Lefebvre, A. H., and Ballal, D. R., *Gas Turbine Combustion: Alternative Fuels and Emissions*, third edit ed., 2010.

[45] Hale, P. L., "A method to estimate weight and dimensions of small aircraft propulsion gas turbine engines," Tech. rep., NASA Lewis Research Center, 1982.

[46] Onat, E., and Klees, W. G., "A method to estimate weight and dimensions of large and small gas turbine engines," Tech. rep., NASA Lewis Research Center, 1979.

[47] McDonald, C. F., "Study of a Lightweight Integral Regenerative Gas Turbine for High Performance," Tech. rep., The Garret Corporation AiResearch Manufacturing Company, Los Angeles, California, USA, 1970.

[48] Shah, R. K., and Sekulic, D. P., *Fundamentals of Heat Exchanger Design*, 2003.

[49] Rodgers, C., "Thermodynamic and Economic Trade Studies for a 3000 kW Gas Turbine." *ASME COGEN*, 1995.

[50] Rodgers, C., "300 kW Class, Semi-Closed Cycle Gas Turbine Engine Design Considerations," *International Gas Turbine & Aeroengine Congress & Exhibition*, ASME, Indianapolis, Indiana, USA, 1999.

[51] Head, A. J., and Visser, W. P. J., "Scaling 3-36kW Microturbines," *ASME TURBO EXPO*, ASME, Copenhagen, Denmark, 2012, pp. 1–9.

[52] Rejman, E., and Rejman, M., "Gears Weight Equation - Gear Chain Weight Calculation Methodology," *MTMVirtual Journals*, , No. 2, 2011, pp. 18–21.

[53] Xu, C., and Amano, R. S., "Empirical Design Considerations for Industrial Centrifugal Compressors," *International Journal of Rotating Machinery*, 2012, pp. 1–15.

[54] Dundas, E. R., "Mechnaical Design of Gas Turbine, in Sawyer's gas turbine engineering handbook," *Turbomachinery International Publications*, Vol. 1, 1985.

[55] Marscher, W. D., "Structural Design and Analysis of Modern Turbomachinery Systems, in Sawyer's gas turbine engineering handbook," *Turbomachinery International Publications*, Vol. 1, 1985.

[56] Tameo, R. W., Vinson, P. W., and Neitzel, R. E., "Regenerative Engine Analysis," Tech. rep., General Electric Company, 1980.

[57] Bettner, J. L., Blandford, C. S., and Rezy, J., "Propulsion System Assessment for Very High Altitude UAV Under ERAST," Tech. rep., Allison Engine Company, Indianapolis, Indiana, USA, 1995.

[58] Hendricks, E. S., "Development of an Open Rotor Cycle Model in NPSS Using a Multi-Design Point Approach," Tech. rep., NASA Glenn Research Center, Cleveland, Ohio, USA, 2011.

[59] Whitfield, A., "Conceptual Design of a Centrifugal Compressor Including Consideration of the Effect of Inlet Prewhirl," *International Gas Turbine and Aeroengine Congress and Exposition*, ASME, Cologne, Germany, 1992.

[60] Groh, F. G., Wood, G. M., Kulp, R. S., and Kenny, D. P., "Evaluation of a High Hub/Tip Ratio Centrifugal Compressor," *Journal of Basic Engineering*, 1970, pp. 419–428.

[61] Aungier, R. H., *Turbine Aerodynamics, Axial-Flow and Radial-Inflow Turbine Design and Analysis*, ASME Press, New York, 2005.

[62] Perdichizzi, A., and Lozza, G., "Design Criteria and Efficiency Prediction for Radial Inflow Turbines," *Gas Turbine Conference and Exhibition*, ASME, Anaheim, California, USA, 1987, pp. 1–9.

[63] Storn, R., "On the Usage of Differential Evolution for Function Optimization," , 1996.

[64] Verstraete, D., and Lunnan, K., "Altitude Effects on the Performance of Small Radial Turbomachinery: Part I —Compressor Impellers," *Proceeding of the ASME Turbo Expo: Power for Land, Sea, and Air*, 2016. URL http://dx.doi.org/10.1115/GT2016-56808.

[65] Verstraete, D., and Lunnan, K., "Altitude Effects on the Performance of Small Radial Turbomachinery: Part II —Turbine Impellers," *Proceedings of the ASME Turbo Expo: Power for Land, Sea, and Air*, 2016, pp. V008T23A015–. URL http://dx.doi.org/10.1115/GT2016-56811.